Computer-aided detection (CAD) of hepatocellular carcinoma on multiphase CT images

Tetsuji TAJIMA*[a], Xuejun ZHANG[a], Teruhiko KITAGAWA[a], Masayuki KANEMATSU[b], Xiangrong ZHOU[a], Takeshi HARA[a], Hiroshi FUJITA[a], RyujiroYOKOYAMA[b], Hiroshi KONDO[b], Hiroaki HOSHI[b], Shigeru NAWANO[c], Kenji SHINOZAKI[d]

[a]Department of Intelligent Image Information, Division of Regeneration and Advanced Medical Sciences, Graduate School of Medicine, Gifu University, Gifu 501-1194, Japan;
[b]Department of Radiology, Gifu University School of Medicine and University Hospital, Gifu 501-1194, Japan;
[c]Department of Radiology, National Cancer Center Hospital East, Chiba 277-8577, Japan;
[d]Department of Radiology, National Kyushu Cancer Center, Fukuoka 811-1395, Japan

ABSTRACT

Primary malignant liver tumor, including hepatocellular carcinoma (HCC), caused 1.25 million deaths per year worldwide. Multiphase CT images offer clinicians important information about hepatic cancer. The presence of HCC is indicated by high-intensity regions in arterial phase images and low-intensity regions in equilibrium phase images following enhancement with contrast material. We propose an automatic method for detecting HCC based on edge detection and subtraction processing. Within a liver area segmented according to our scheme, black regions are selected by subtracting the equilibrium phase images to the corresponding registrated arterial phase images. From these black regions, the HCC candidates are extracted as the areas without edges by using Sobel and LoG edge detection filters. The false-positive (FP) candidates are eliminated by using six features extracted from the cancer and liver regions. Other FPs are further eliminated by opening processing. Finally, an expansion process is applied to acquire the 3D shape of the HCC. The cases used in this experiment were from the CT images of 44 patients, which included 44 HCCs. We extracted 97.7% (43/44) HCCs successfully by our proposed method, with an average number of 2.1 FPs per case. The result demonstrates that our edge-detection-based method is effective in locating the cancer region by using the information obtained from different phase images.

Keywords: Multislice CT, Computer-aided diagnosis and detection (CAD), Edge extraction, Subtraction method

1. INTRODUCTION

Hepatocellular carcinoma (HCC) is prevalent in Asia and Africa. Although HCC is not prevalent in North America at present, the number of HCC cases may increase in the near future because there is a large subclinical population with hepatitis C virus infection. According to a report in the New England Journal of Medicine published in 1999, HCCs in the United States increased from 1.4 to 2.4 persons per 100,000 people from the period between 1976 and 1980 to that between 1991 and 1995. Additionally, the mortality rate from primary liver cancer is said to have increased by 41% and the proportion of hospitalizations due to this disease increased by 46% during the last two decades. Early detection and accurate staging of HCC is an important concern in practical radiology. Currently, although multidetector-row computed tomography (MDCT) is widely used for the diagnosis of liver tumors, information obtained from CT is very large, and it is difficult for inexperienced radiologists or physicians to interpret all of the CT images in a short time. The purpose of our study is to establish a computer-aided diagnosis system for aiding decision with regard to the diagnosis of HCC by using multiphase CT images.

Okumura et al. developed a computer-aided temporal and dynamic subtraction technique of the liver for the detection

*fujita@fjt.info.gifu-u.ac.jp; phone (+81) 58-230-6512; (+81) 58-230-6514

Medical Imaging 2007: Computer-Aided Diagnosis, edited by Maryellen L. Giger, Nico Karssemeijer,
Proc. of SPIE Vol. 6514, 65142Q, (2007) · 1605-7422/07/$18 · doi: 10.1117/12.709174

of small HCCs on abdominal CT images[1]. By using dynamic images obtained by subtracting non-enhanced CT images from arterial phase CT images of the liver obtained at the same position, the nodule-to-liver contrast was increased by 150%. However, HCC is detected by a radiologist, and the requiring status of breath for a patient during CT scanning is very high due to the simple registration method only using affine transformation on the two different time series images, particularly if the tumor is smaller than 10 mm. Other researches on the automatic extraction of liver tumors on MDCT images have already been reported by Nakagawa et al.[2] and Hayashi et al.[3]. They used the technique of free-form deformations (FFD) for the registration of CT images obtained in two different phases, which is the same technique reported by Rivers[4]. It is possible to obtain a highly accurate registration with FFD, but the processing time is very long. In order to use a CAD system in real clinical practice, limiting the running time of CAD to an acceptable degree has to be considered. In our study, thin-plate splines (TPS) have been used for the registration of time series images. TPS can also transform images by non-rigid registration as FFD, but its time cost is very small. We have developed a CAD system for the detection of HCC on multi-phase CT images based on the density change in the liver and HCC areas caused by the effects of the contrast agent. Our method consists of six steps: (1) reducing noises using a median filter, (2) registration of images using TPS, (3) extraction of liver, (4) extraction of HCC candidate areas using subtraction processing and edge detection, (5) eliminating false-positive (FP) candidates using six features, and (6) expansion of the HCC candidate area.

2. MATERIALS AND METHODS

2.1 Abdominal CT images of the liver and HCC

Typically, HCCs show rich arterial neovascularization with a decrease in the portal supply. Therefore, multidetector row helical phase CT is routinely used in Japan in the detection of HCC in patients. In order to determine which phases are fit for a CAD study, a quadruple-phase protocol that included unenhanced, hepatic arterial, portal venous, and delayed phases was performed by using an MDCT scanner (Aquilion; TOSHIBA, Japan). Each patient received a Contrast/Bolus Agent (Oypalomin370 or Optiray320) by means of a power injector at a rate of 3 mL/s, and the ensuing average volume of the contrast material was equal to 100 mL (range, 110–182 mL). Four complete acquisitions of the entire liver were obtained in a craniocaudal direction during one breath hold with the following parameters: slice interval, 0.625–1.25 mm; number of bits stored, 16; pixel-spacing, 0.50–0.625 mm; spatial resolution, 512 × 512; 165 effective mAs; and 120 kVp. In all patients, non-contrast scanning (i.e., the first pass) was performed. The ensuing average start time for the hepatic arterial phase was 37 s (range, 35–40 s). The scans obtained in the portal venous phase and the equilibrium phase (i.e., the third and fourth passes, respectively) were acquired at 65 s (range, 60–70 s) and 180 s, respectively, after the initiation of contrast material injection.

Although the unenhanced images do not confer a significant advantage in terms of HCC detection because of the small difference in tumor and liver attenuation, as shown in (Fig. 1(a), such phase images can play an important role in the detection and differentiation of uncertain lesions (such as cysts, regenerative nodules, focal confluent fibrosis, small intraparenchymal calcification, and focal sparing of fatty infiltration) from HCC nodules. During the arterial phase, aortic

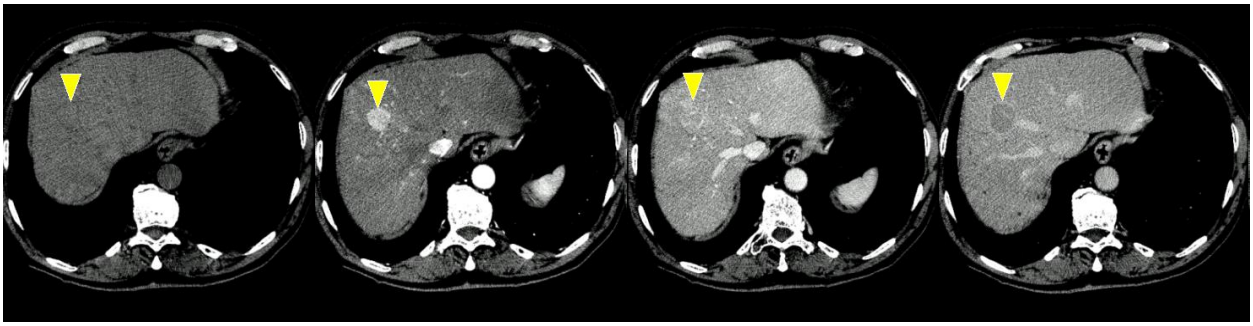

(a) (b) (c) (d)

Fig. 1 MDCT images obtained in four phases: unenhanced images (a); arterial phase image (b); portal venous image (c); and equilibrium phase image (d).

and hepatic arterial enhancement increases rapidly and quickly peaks after the end of the injection. The effects of arterial enhancement are seen approximately 35–40 s after the initiation of contrast injection. Because the liver receives most of the blood from the portal system, hepatic parenchyma enhancement lags behind arterial enhancement. HCCs are typically hyperattenuating on hepatic arterial phase images, and the portal veins were also enhanced at this phase (Fig. 1(b)). Approximately 60–70 s after the initiation of injection, arterial enhancement decreases, and parenchymal enhancement increases because of portal venous inflow. Liver is enhanced in the portal venous phase because it receives little blood from arteries, but a considerable amount of blood from the portal vein. The intensity of HCCs decreases and their appearance changes from hyperattenuating nodules to hypoattenuating nodules. In the portal venous phase, HCCs may be shown as regions having an intensity lower than or same as that of the liver (Fig. 1(c)). The liver, hepatic veins, and portal veins are all enhanced in this phase; therefore, this phase is widely used for the simulation of liver resection or living donor liver transplantation. The equilibrium phase images are obtained at 3 min after the injection of the contrast agent. The effect of the contrast agent is preserved in the whole liver, but the density of HCCs decreases and they appear darker than the liver area (Fig. 1(d)).

The cases used in this experiment are from the multidetector row CT (MDCT) 3D images of 44 patients; these were provided by National Cancer Centre Hospital East, Japan. Each case includes sequence images obtained in four phases; these images were scanned before and after injecting the enhancement material at 0, 30, 60, 120 s. The categories of these cases were confirmed by an experienced radiologist; the cases included 12 normal cases and 32 cancer cases with a total of 44 HCC tumors.

2.2 Outline of processing

Figure 2 shows the flowchart of the extraction of HCC. The original multiphase images are firstly preprocessed by resampling to half size, smoothing by median filter, and a landmark-based registration. Secondly, the HCC candidate regions are extracted within the liver area by subtraction and edge detection methods, and FP detections are eliminated by using six extracted features. Finally, the HCC is reshaped by region growing.

2.3 Registration of multiphase images

The proposed method in this study uses CT images obtained in two or more phases. The dataset of images in each phase is obtained in a sequence according to different time settings after the contrast agent is injected. Therefore, if the patient

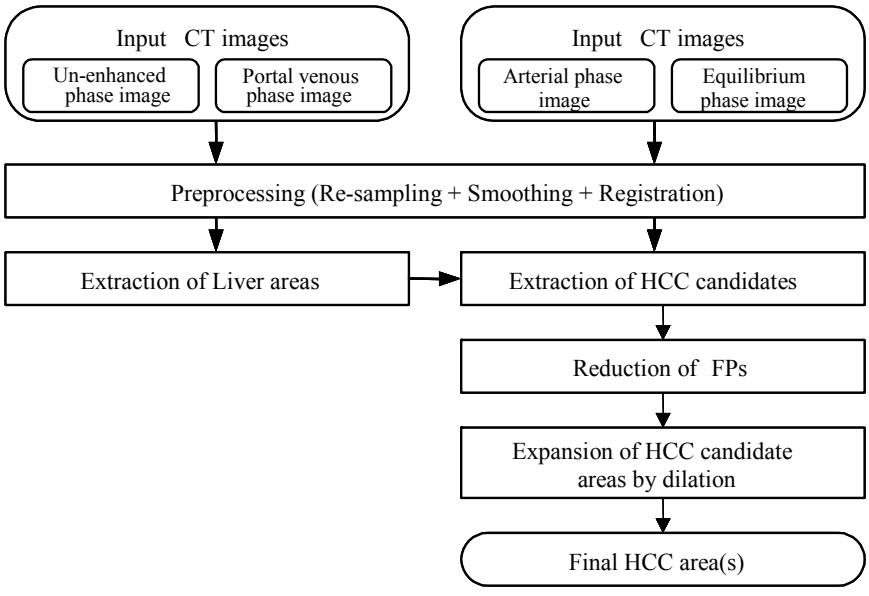

Fig. 2 The overall flowchart of the extraction of HCC.

moves his body or changes the status of breath during the whole scanning time, misregistration might occur between the images of each phase. This will greatly influence the result obtained by our method since HCC candidates are extracted based on the combined imaging information obtained from different time series images on MDCT. Therefore, it is necessary to align the image space of one image to that of the other. Such processing is-called intramodal registration and can reduce this influence by the deformation of organs in images obtained at different times.

In our study, thin-plate splines (TPS) were used for the registration. TPS is a technique for transforming the image by moving the control point[5]. The image can be transformed by setting the coordinates of the control point before and after the image moves. Moreover, users need not worry about the order of the control point in this technique, making it convenient to use.

$I(x, y, z)$ is defined as the fixed image and the other as moving image $I'(x', y', z')$, where x, y, and z represent a position in 3D volumes. TPS registration attempts to determine an alignment spatial mapping between two images by moving the control point (x_i, y_i, z_j) on the moving image to the corresponding control point (x'_i, y'_i, z'_j) on the fixed image, where $1 \le i \le n$, $1 \le j \le m$. The moving image obtained after transformation by using TPS can be expressed by the following equations:

$$I(x', y', z') = I(f_x, f_y, f_z) \tag{1}$$

and

$$\begin{cases} f_x(x,y,z) = a_{11} + a_{1x}x + a_{1y}y + a_{1z}z + \sum_{i=1,j=1}^{n} w_{1i} U(\|(x,y,z) - (x_i, y_i, z_j)\|) \\ f_y(x,y,z) = a_{21} + a_{2x}x + a_{2y}y + a_{2z}z + \sum_{i=1,j=1}^{n} w_{2i} U(\|(x,y,z) - (x_i, y_i, z_j)\|) \\ f_z(x,y,z) = a_{31} + a_{3x}x + a_{3y}y + a_{3z}z + \sum_{i=1,j=1}^{n} w_{3i} U(\|(x,y,z) - (x_i, y_i, z_j)\|) \end{cases} \tag{2}$$

Coefficient a, w, and $U(r)$ are calculated as stated below:

$$\begin{bmatrix} \mathbf{w} \\ \mathbf{a} \end{bmatrix} = \begin{bmatrix} \mathbf{V} \\ 0 \end{bmatrix} \begin{bmatrix} \mathbf{K} & \mathbf{P} \\ \mathbf{P}^T & 0 \end{bmatrix}^{-1} \tag{3}$$

and

$$U(r) = |r|, \tag{4}$$

where

$$\mathbf{P} = \begin{bmatrix} 1 & x_1 & y_1 & y_1 \\ 1 & x_2 & y_2 & z_2 \\ \dots & \dots & \dots & \dots \\ 1 & x_n & y_n & z_n \end{bmatrix}, \qquad \mathbf{V} = \begin{bmatrix} x_1' & x_2' & \dots & x_n' \\ y_1' & y_2' & \dots & y_n' \\ z_1' & z_2' & \dots & z_n' \end{bmatrix}, \qquad \mathbf{K} = \begin{bmatrix} 0 & U(r_{12}) & \dots & U(r_{1n}) \\ U(r_{21}) & 0 & \dots & U(r_{2n}) \\ \dots & \dots & \dots & \dots \\ U(r_{n1}) & U(r_{n2}) & \dots & 0 \end{bmatrix}.$$

Eleven landmarks are selected manually on the artery phase images to obtain a fixed image (Fig. 3), and the corresponding points in the images obtained in other phases are also selected. These are as follows: one point at the centroid of the liver region that first appeared on the top slice near the heart (P1); four points on the abdominal wall at the P1 slice axial plane (P2–P5); one point outside the lateral segment on the left lobe (P6); one bottom point at the

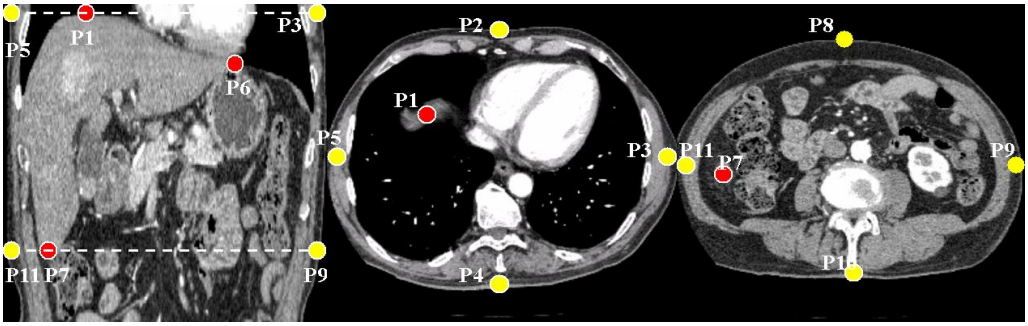

(a) (b) (c)

Fig. 3 Control points selected for TPS on the coronal plane (a); Axial-plane slice showing that the liver region first appeared on the top slice near the heart (b); axial plane image of the bottom point at the posterior segment (caudal part) on the right lobe (c).

posterior segment (caudal part) on the right lobe (P7); four points on the abdominal wall at this P7 slice axial plane (P8–P11).

2.4 Extraction of liver area

We have been developing an automatic method for the segmentation of the liver region on multislice MDCT and MR images[6], which is based on the edge detections by using Sobel and LoG filters on the subtraction image of noncontrast and portal venous phase images. The following steps of detecting HCC are only undertaken in the extracted liver area (Fig. 4) in order to decrease the FP detection.

2.5 Extraction of the HCC candidate

2.5.1 Subtraction processing

The HCC is shown as a high-intensity region in the arterial phase image (Fig. 5(a)) and a low-intensity region in the equilibrium phase image (Fig. 5(b)) due to the effect of the enhancement material. This feature is used for the extraction of HCC by subtracting the equilibrium phase image from the arterial phase image. The pixels on the subtraction image are converted to 0 if their intensity is below 0, in which case, the image is regarded as the HCC candidate, as shown in Fig. 5(c).

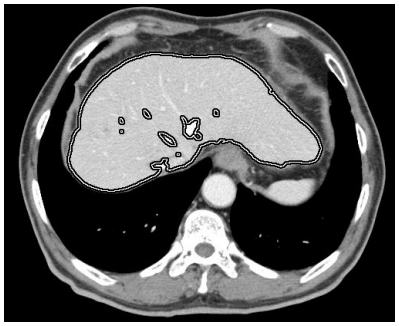

Fig. 4 An extracted liver contour is drawn by the black lines.

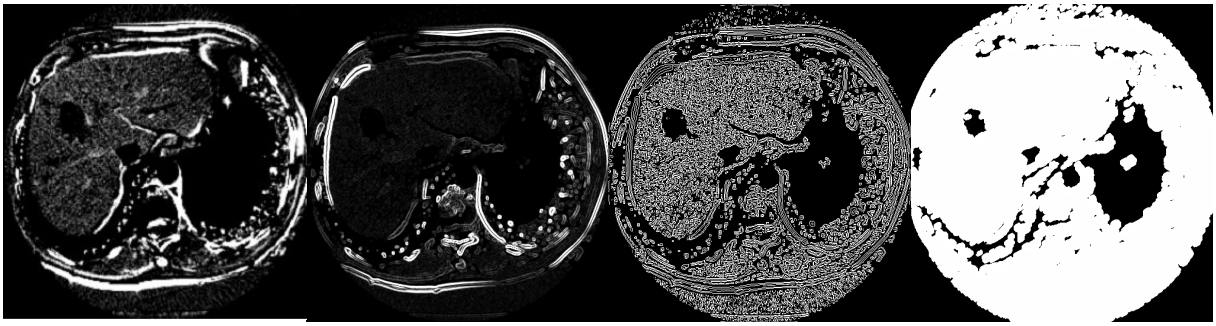

(a) (b) (c) (d)

Fig. 5 Extraction of HCC candidates is performed by subtracting the equilibrium phase image from the arterial phase image. The edge of the HCC is lost in the subtraction map (a) after edge detection by Sobel filter (c) and LoG filter (b), and the candidate can be extracted from the expanded image(d).

2.5.2 Detection of edges

The edges (Fig. 5(d)) are detected by using the Sobel and LOG filter from the subtraction image, and the area without the edges within the liver area is detected as an HCC candidate area.

2.6 Elimination of FPs

Many non-HCC areas are included among the candidates extracted by the method described in section 2.5. These FPs are eliminated by the following step. An FP with small region is deleted by opening processing in which the structural element is below two pixels in radius. Six features obtained from the cancer candidate area are used for FP elimination. These include four features (sphericity, volume, average density at arterial phase, and average density at equilibrium phase) in the HCC candidate and two features (average density difference between the HCC candidate and the liver region in the arterial phase and equilibrium phase images). FPs are eliminated by the rule-base method using each feature, as shown in Fig. 6.

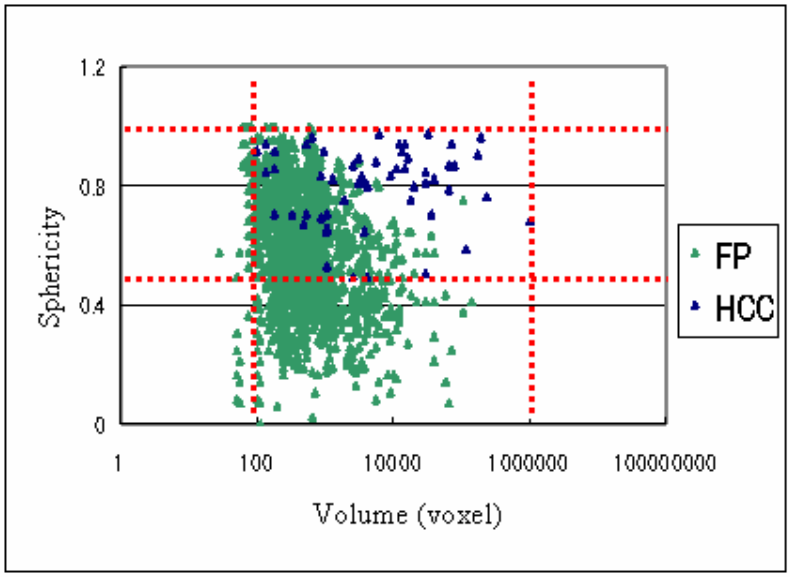

(a)

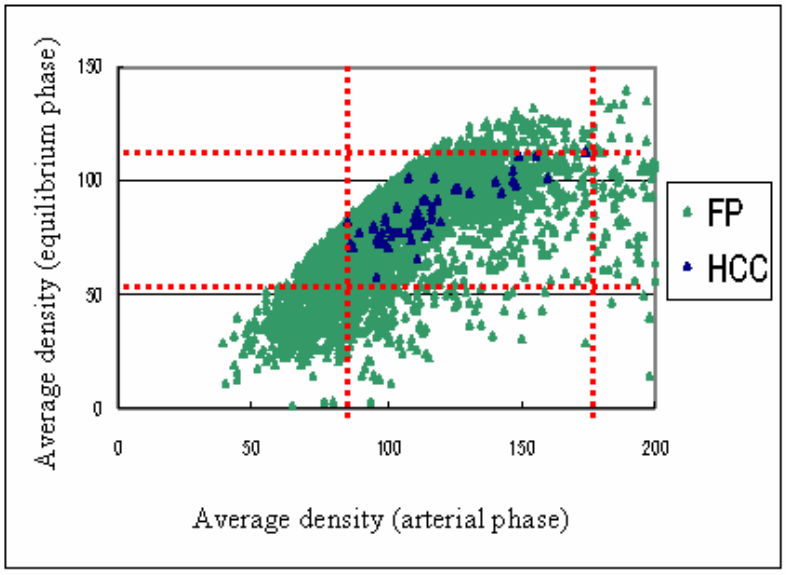

(b)

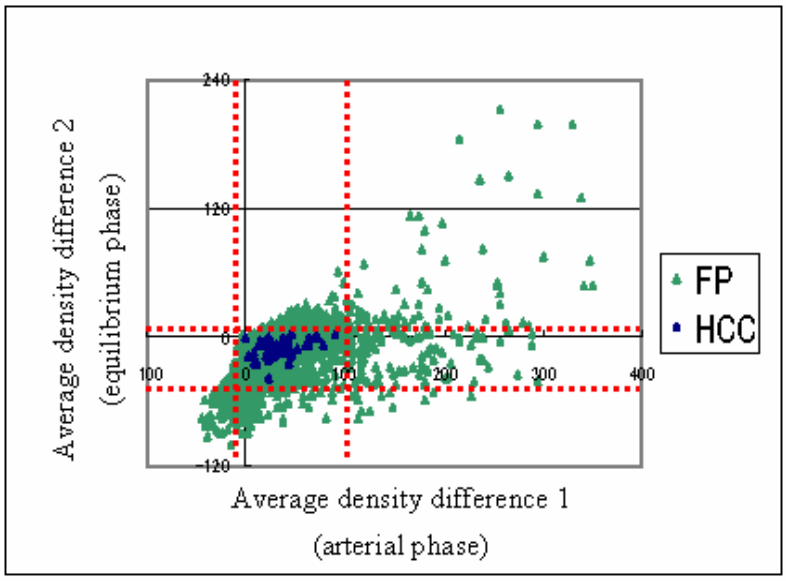

(c)

Fig. 6 Six features obtained from the cancer candidate area are used for false-positive elimination by rule-based method, according to the HCC-FP distribution in (a), (b) and (c). Note that Average density difference 1 is average density difference between the HCC candidate and the liver region in the arterial phase. Average density difference 2 is Average density difference between the HCC candidate and the liver region in the equilibrium phase.

2.7 Expansion of the HCC candidate area

Because only a part of the tumor is extracted as the candidate area obtained by the above step (Fig. 7(a)), expansion

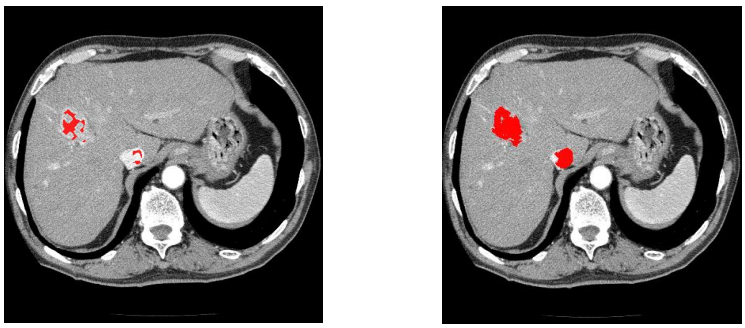

(a) (b)

Fig. 7 The final region of HCC (b) is obtained by the region growing method on the extracted candidate regions (a).

processing is applied to acquire the shape of the HCC by using the regional density information (Fig. 7(b)). Each time, a candidate region *R1* is expanded by three pixels in radius to obtain a new region *R2*. The difference region *R3* is equal to *R2 – R1*. This expansion processing is repeated till the average gray value in the *R3* region on the arterial phase image *G1r3* and on the equilibrium phase image *G2r3* satisfies the condition of $G1r3 < G2r3$.

3. RESULT AND DISCUSSION

The performance of our program was evaluated by detecting HCC tumors with all sizes. We extracted 97.7% (43/44) of the HCC tumors successfully by our proposed method with 5.8 FPs per patient.

Figure 8 shows four example results of the HCC extraction, where the HCCs detected by our method are outlined by dark closed lines. Two cancer regions were accurately detected in Fig. 8(a) and Fig. 8(b), but a part of HCC was lost in Fig. 8(a) due to the failure in the process of expanding the HCC candidate area. Some FPs were missed in some hepatic vessels (Fig. 8(c)) or the area near the liver contour. This may be caused by misregistration of the liver regions or by a part of vein being extracted after the subtraction method. Future research should focus on the improvement of the accuracy of registration and the addition of new features for FP elimination. One TP was lost because of its intensity was similar to that of the liver region ((Fig. 8(d)) and it could not be detected in the subtraction processing. Using an

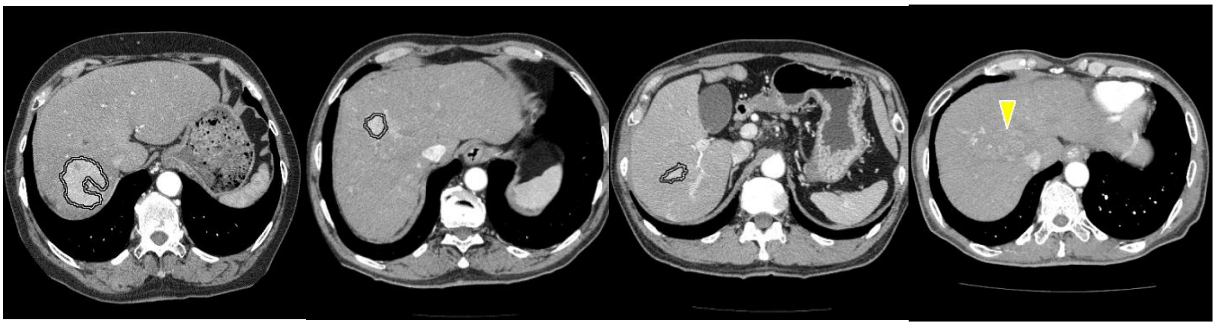

(a) (b) (c) (d)

Fig. 8 Two successful examples with outlining the extracted HCC contour in (a) and (b). Two false examples of a false extraction with a part of hepatic vessel (c) and a missed detection of TP (arrow) (d).

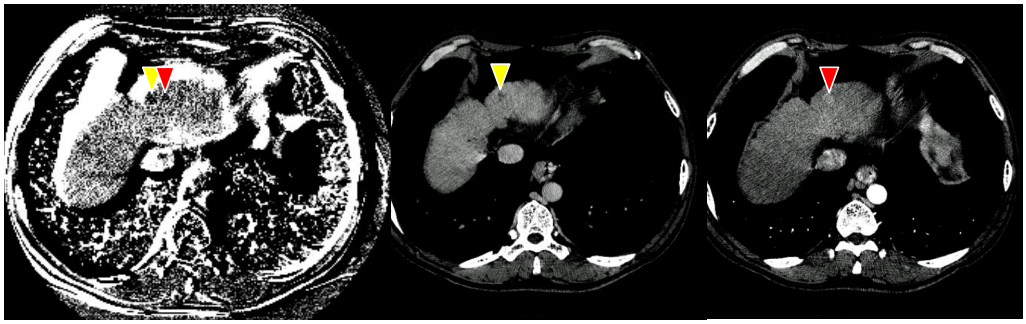

(a) (b) (c)

Fig. 9 The position of cancer (arrow) is not identical on the overlap map (a) that integrated from the equilibrium phase image (b) to the arterial phase image (c).

enhancement technique may improve the detection of such cases.

Although our affine-based registration method was useful for liver segmentation, the position of cancer in arterial phase images might be different from that in equilibrium phase images when only using rigid transformation is used (Fig. 9(a)). In particular, if the tumor is small in size, the subtraction process (Fig. 9(b) and Fig. 9(c)) cannot enhance the cancer region in the same position. Therefore, the small HCC candidate was eliminated as FP after edge detection. Detection of this HCC became possible by using the non-rigid transformation method TPS in this study, even if the patient changed the durations of breath holds frequently during the period when scanning is performed twice. Therefore, our landmark-based method for registration is effective, and automatic acquisition of the control points is difficult in the next step. In addition, in this experiment, FPs are eliminated using six features by the rule-based method. Other efficient classifiers such as support vector machine (SVM) or artificial neural network (ANN) will be used for further improvements.

4. CONCLUSIONS

In this paper, an automatic method is proposed for the extraction of the HCC region on multislice MDCT images. The result demonstrates that our edge detection-based method is effective in locating the cancer region by using the information collected from images obtained in different phases. Future research should focus on improving the TP rate and decreasing the number of FPs. Moreover, the registration of images obtained in different phases will be helpful to extract small HCC tumors.

5. ACKNOWLEDGMENTS

This research was supported in part by the Ministry of Health, Labour, and Welfare under a Grant-In-Aid for Cancer Research and in part by the Ministry of Education, Culture, Sports, Science and Technology under a Grant-In-Aid for Scientific Research, Japanese Government. The author T. Tajima would like to express his appreciation to Research Foundation for the Electrotechnology of Chubu for their finance support on the project.

REFERENCES

1. E. Okumura, S. Sanada, M. Suzuki, and O. Matsui, “A computer-aided temporal and dynamic subtraction technique of the liver for detection of small hepatocellular carcinomas on abdominal CT images.” Phys. Med. Biol. Vol.51, pp.4759–4771, 2006.

2. J. Nakagawa A. Shimizu, and H. Kobatake, “Development of an automated extraction method for liver tumors in three-dimensional multiphase multislice images,” Systems and Computers in Japan, Vol.36, no.9, pp.43–54, 2005.
3. Y. Hayashi, D. Deguchi, T. Kitasaka, K. Mori, Y. Mekada, and Y. Suenaga, “Detection of liver cancer regions from dynamic CT images,” International Journal of Computer Assisted Radiology and Surgery (CARS2006), Vol.1, Supplement 1, H. U. Lemke, K. Inamura, K. Doi, M. W. Vannier, and A. G. Farman (Eds.), pp.524–525, 2006.
4. J. Rivers, D. Rueckert, L. I. Sonoda, C. Hayes, D. L. G. Hill, M. O. Leach, and D. J. Hawkes. “Non-rigid registration using free-form deformations: application to breast MR images,” IEEE Trans. on Medical Imaging, Vol.18, no.8, pp.712–721, 1999.
5. F. L. Bookstein, “Principal warps: Thin-plate splines and the decomposition of deformations,” IEEE Trans. on Pattern Analysis and Machine Intelligence, Vol. 11, no. 6, pp.567–585, 1989.
6. X. Zhang, W. Li, H. Fujita, M. Kanematsu, T. Hara, X. Zhou, H. Kondo, and H. Hoshi, “Automatic segmentation of hepatic tissue and 3D volume analysis of cirrhosis in multi-detector row CT scans and MR imaging,” IEICE, Vol.E87-D, no.8, pp.2138–2147, 2004.